Squeezing red blood cells on an optical waveguide to monitor cell deformability during blood storage

Balpreet Singh Ahluwalia[1] *, Peter McCourt[2], Ana Oteiza[2], James S. Wilkinson[3], Thomas R. Huser[4] and Olav Gaute Hellesø[1]*

[1]Department of Physics and Technology, University of Tromsø, N-9037 Tromsø, Norway
[2]Department of Medical Biology, University of Tromsø, N-9037 Tromsø, Norway
[3]Optoelectronics Research Centre, University of Southampton, SO17 1BJ, UK
[4]Department of Physics, University of Bielefeld, Bielefeld, Germany

*Corresponding Authors: balpreet.singh.ahluwalia@uit.no and olav.gaute.helleso@uit.no

Supplementary information

Supplementary Movies

Supplementary Movie 1: Optical trapping of a red blood cell on a 2 μm wide waveguide. When the laser is switched on, the cell is attracted towards the waveguide and deforms. The cell regains its original shape and size when the laser is switched off.

Supplementary Movie 2: Optical trapping and propulsion of red blood cells on an optical waveguide of width 10 μm. No structural deformation of the cell is observed when a cell is trapped on a waveguide wider than the diameter of the cell.

Supplementary Movie 3: Optical trapping and propulsion of red blood cells on a 4 μm wide waveguide. When the laser is switched on, the trapped cells are laterally deformed on a waveguide and are propelled along the waveguide. When a squeezed cell is propelled along the waveguide, the distribution of optical forces will change, causing the cell to readjust. Moreover, as the waveguide is multimode, mode beating along the waveguide will also influence the cell squeezing as the cell moves along the waveguide.

Supplementary Movie 4: Squeezing of cells on an optical waveguide is a planar technique and works simultaneously on a large number of cells. The movie shows optical trapping of red blood cells on a tapered waveguide (8 to 1 μm). The tapered waveguide is shown in Supplementary Fig. 1. The cells trapped on a narrow section (1.3 μm) were squeezed, while cells trapped on a wide section (8 μm) were propelled without any structural deformation. An objective lens with lower magnification (Olympus 20X, NA 0.4) was used to have a larger field of view and thus image more cells. The objective lens is moved to image the various sections along the waveguide.

Waveguide fabrication and experimental apparatus

The fabrication steps and optimization can be found in Ref. [1]. The taper was made by sharply reducing the width from 8 μm to 1.3 μm as shown in Supplementary Figure 1. The narrow section was later enlarged back to 8 μm width, such that both the input and output facets of the waveguide were wide (8μm). Coupling and propagation losses were estimated to be 15 dB for a 3 cm long and 180 nm thick waveguide. For 500 mW incident on the waveguide, the guided power at the trapping location was estimated to be in the range of 10-20 mW for the tapered waveguide. For simulation we used guided power of 15 mW, as discussed below.

The flow chamber was made of PDMS and its thickness varies between 500-1500 μm. A thin layer of PDMS was grown separately and then pasted on top of waveguide chip. A small rectangular section of PDMS was removed (opened) to access the waveguides. The cell was introduced onto the waveguides from top of this opening (rectangular section) and the PDMS chamber was then sealed with a cover slip. As sample was closed, evaporation was not a problem for the experiment durations (1-3 hours). After the experiments coverslip and PDMS chamber was removed and chip was thoroughly cleaned using Isopropanol, Ethanol and water (ultrasonic cleaning).

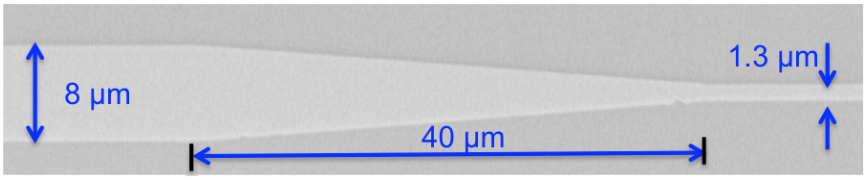

Supplementary Figure 1. Optical image of a tapered waveguide used for squeezing of red blood cells.

The schematic diagram of the experimental apparatus is shown in Supplementary Figure 2 and in Ref [2].

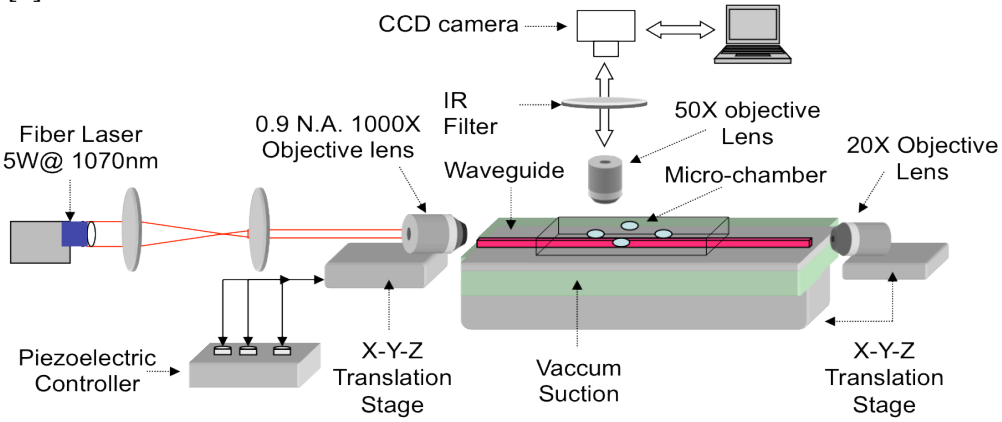

Supplementary Figure 2. Experimental set-up for waveguide trapping.

Waveguide cell squeezing

Supplementary Figure 3 (similar to Fig. 2 of the manuscript) shows optical squeezing of a red blood cell on a 1.3 μm wide waveguide. When a cell arrives at the waveguide, it is trapped at the edge and is held in place while the other bulges of the cell (lying outside the waveguide) squeezes. The part of the cell that is overlapping with the waveguide straightens and its length increases slowly from 4.4 μm to 6.7 μm (Supplementary Figure

3(b-g)). The length of the squeezed cell remains at 6.7 µm (Supplementary Figure (3e-g)), which is slightly smaller than the length of the unsqueezed cell (7 µm, Supplementary Figure 3(a)). This experimental observation is in coherence with the simulation that predicts a strong downwards pull and a straightening effect on the part of the cell that is overlapping with the available evanescent field of the waveguide (Figure 6). During the initial stages (Supplementary Figure 3(b-f)), as the cell is pulled towards the waveguide and squeezed, the outer periphery (bulge) of the blood cell becomes darker, suggesting an increase in thickness. The central part of the donut remains transparent (thin), but decreases in size (Supplementary Figure 3(b-e)).

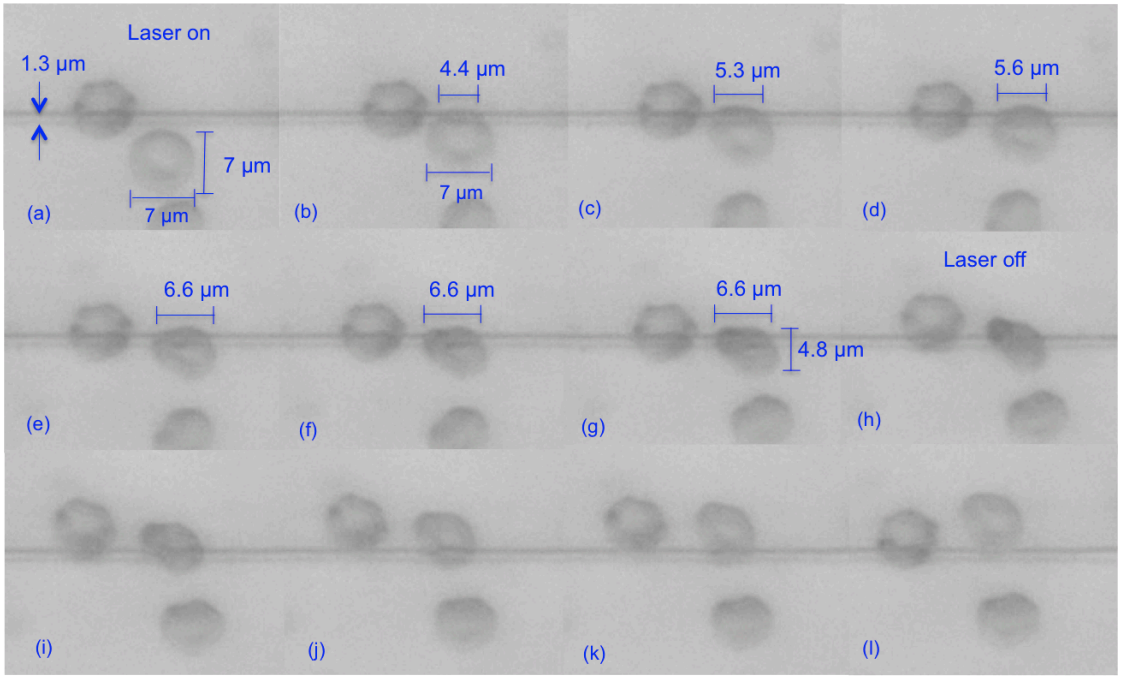

Supplementary Figure 3. (a-g) Optical squeezing of a red blood cell on a 1.3 µm wide waveguide, (h-l) the trapped cell regains its donut shape when laser is switched off. Associated movie 1.

Supplemenatry Figure 4 shows optical squeezing of a cell with high deformability (DI> 0.4) as shown in Fig. 3d. The squeezing of cells starts in the similar manner, i.e. the edge of the cell is attracted onto the waveguide and is straightened, as shown in Supplementary Fig. 4(a-c). The central donut of the cell is faintly visible till c), however, it is difficult to interpret what happens subsequently, i.e. after Supplementary Figure 3(d), from two-dimensional images. For this case, the rim of the cell is either very closely squeezed or the cell might have rotate at the edges.

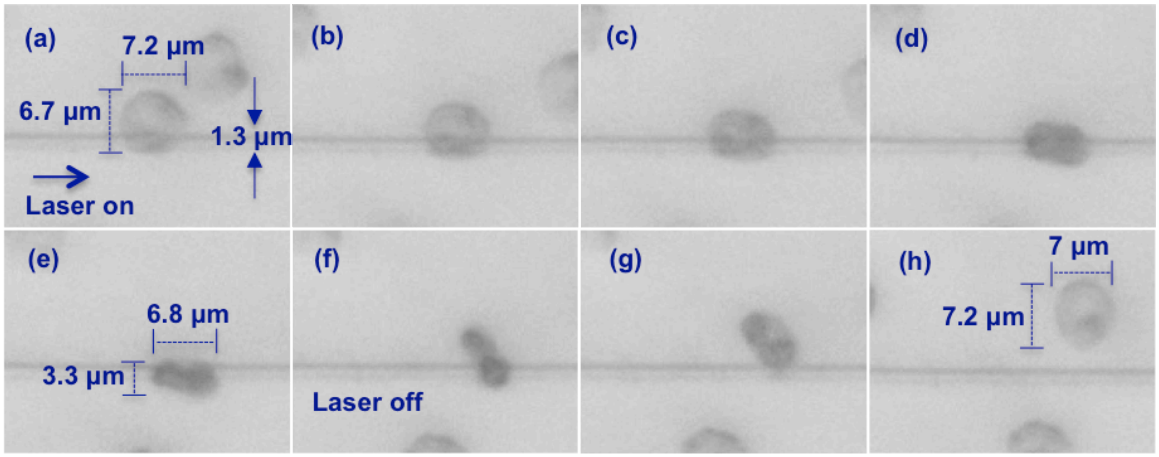

Supplementary Figure 4. Optical squeezing of a red blood cell on a 1.3 µm wide waveguide. The cell shown is one of the cases with high deformability, DI>0.4.

Numerical simulations with the finite element method

The force density $\boldsymbol{f}$ on a non-magnetic, isotropic dielectric body in an electromagnetic field is [3, 4]:

$$\boldsymbol{f} = -\frac{1}{2}\epsilon_0 E^2 \nabla\epsilon, \quad (1)$$

with ε_0 denoting the electric permittivity of vacuum, E the electric field and $\nabla\varepsilon$ the permittivity gradient. Optical forces and optical pressures were simulated with the software Comsol Multiphysics (version 4.3a). Simulations of a full-size cell (7µm diameter) were run on a computer cluster, using four to eight nodes with 128 GB memory each [5]. The parameters for the laser, waveguide thickness (180 nm) and width (1.3 µm and 3 µm), guided power and the cell were kept similar to the experiments. The input power was set to 1mW at a wavelength of 1070 nm, with all results scaled up to 15 mW in post-processing (Figure 5-8 of the main paper). All calculated forces and pressures are linear with the guided laser power. Cells were taken to be biconcave according to Ref. [6, 7], but with a diameter of 7 µm to match the experimentally observed size. For the refractive index of the cells, a value of n = 1.4 was used [8].

The fundamental mode of the waveguide was first computed in two dimensions for TE-polarization, before leaving the field to propagate into a full three-dimensional model. The waveguides considered have at least one TM-mode and two TE-modes according to the simulations, whereas only the fundamental TE-mode was observed experimentally for a waveguide width of 1.3 µm. A perfectly matched layer (PML) was used at the end-face of the model, while scattering boundary conditions were used on the sides, top and bottom of the model. The cell is kept at a separation of 5 nm above the surface of the waveguide to simplify the simulations, at the expense of a slight variation in the calculated optical force. The model was tested for numerical stability using various settings. A separation of 5 nm was compared with a separation of 2 nm using a finer mesh. The effect of separation and mesh was tested for the cell displaced 2.6 µm from the centre of a 1.3 µm wide waveguide (close to maximum magnitude of forces, see Fig 5). The combined effect of reducing the separation and using a finer mesh was found to be less than 6% for F_x and F_y.

The F_x and F_y components of the optical force were found by integrating the Maxwell stress tensor T over the cell surface S [9-10]:

$$\vec{F} = \oint_S \overleftrightarrow{T} \cdot \hat{n}\, dS. \quad (2)$$

The outwardly directed unit normal on the surface is given by $\vec{n}$. Local optical pressure can also be found from the Maxwell Stress Tensor by taking the difference between the diagonal radial components on the two sides of the surface (i.e. cell membrane) [4]. We found this to give too high numerical noise, and rather computed the pressure σ from the tangential field component E_t and the radial field component E_r, again according to [4]:

$$\sigma^{AM} = \frac{1}{4}\varepsilon_0 n_w^2 \left(\frac{n_c^2}{n_w^2} - 1\right)\left[E_t^2 + \frac{n_c^2}{n_w^2}E_r^2\right]_{a-}, \quad (3)$$

with the refractive index of the cell n_c = 1.4, the refractive index of water n_w = 1.33 and the index *a*- indicating that the radial field component is taken inside the membrane. Comsol use a complex representation of the field, which gives the factor 1/4 in front, while a real field is used in [9] with a factor 1/2. Eq. (3) is the Abraham-Minkowski part of the pressure. By integrating the pressure multiplied by a component of the surface normal, e.g. n_x, the corresponding force component (F_x) on the cell is found:

$$F_x = \oint_S \sigma^{AM} \cdot n_x \, dS. \quad (4)$$

The results for F_x found with Eq. (2) and Eq. (4) were within 4% for a lateral offset y < 3.2 μm, increasing to 8% for y > 3.4 μm as the magnitude of F_x decreased.

In order to study the influence of the waveguide width on trapping, we fixed the thickest part of the cell in the centre of the waveguide. For Figure 7 (in the main paper), this corresponds to fixing the edge of the white circle on the centreline of the waveguide, giving a fixed offset of 2.45 μm for a cell diameter of 7 μm. For this configuration, the force components F_x and F_y as a function of the waveguide width are shown in Supplementary Figure 5. The bottom of the cell is 10 nm above the top of the waveguide, whereas it is 5 nm for the other figures. This reduces the required mesh size, which was an advantage for the large waveguides, but also reduces the forces by about 10%. An increase of the waveguide width reduces both forces, with a sharper reduction for the lateral force F_y than for the vertical force F_x. A narrow waveguide is thus crucial to pull the cell sideways and down onto the waveguide.

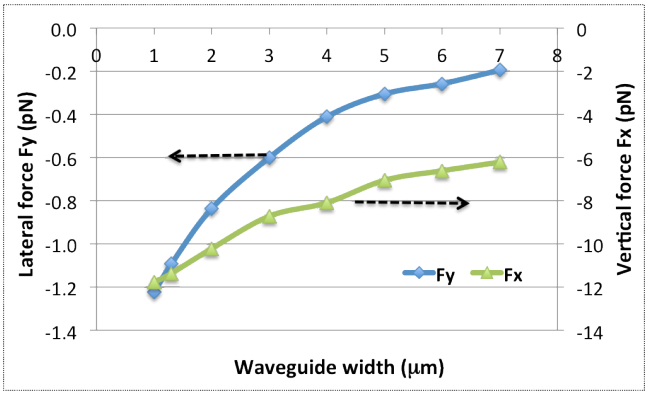

Supplementary Figure 5. Forces on a cell with the rim fixed in the centre of the waveguide (i.e. offset 2.45 μm) as a function of waveguide width. The bottom of the cell is 10 nm above the top of the waveguide, whereas it is 5 nm for the other figures.

The distribution of forces on the cell gives a torque. The torque τ is given by [11]:

$$\tau = \oint_S (\vec{r} \times \overleftrightarrow{T}) \cdot \hat{n}\, dS, \tag{5}$$

with $\vec{r}$ giving the distance from the axis of rotation to a point on the surface of the cell. The expression is thus similar to eq. (2) used for the force. It is necessary to define the axis of rotation, which will be given by the (extreme) point(s) of contact between the cell and the surface (waveguide or substrate). When the bulge of the cell is on the waveguide, the axis of rotation will be given by the bottom of the bulge, as marked with a white arrow in Fig. 6b). This is the case for an offset > 1.8 μm (radius of bulge minus half the waveguide width). For a smaller offset, the axis of rotation will, strictly speaking, be the intersection of the waveguide edge with the bottom of the cell. However, if the cell rotates or deforms slightly, the bulge will get in contact with the substrate and the bottom of the bulge (white arrow in Fig. 6b) will again define the axis of rotation. We have thus calculated the torque relative to an axis of rotation through the bottom of the bulge (again, white arrow in Fig. 6b) for all offsets. The direction of the torque is given in Fig. 1a). For a positive torque, the cell will be pressed down to the waveguide and the substrate, whereas for a positive torque it will rotate upwards, away from the substrate, with its bulge on the waveguide. The calculated torque is given in Figure 8 in the manuscript.

Supplementary Figure 6 shows the pressure on cells trapped at the stable position (laterally) for waveguides of width a) 1.3 μm and b) 3 μm. As the input power is distributed over a larger waveguide width and the field is varying more slowly across the waveguide, the pressure is significantly reduced for the wider waveguide. Supplementary Figure 7 shows the distribution of pressure on a cell trapped on a 1.3 μm wide waveguide at the stable position (offset =2.1 μm). The evanescent field is prominent only upto 150 nm from the waveguide surface, thus it creates a localized pressure on the part of the cell surface overlapping with the evanescent field (see Supplementary Fig. 7b).

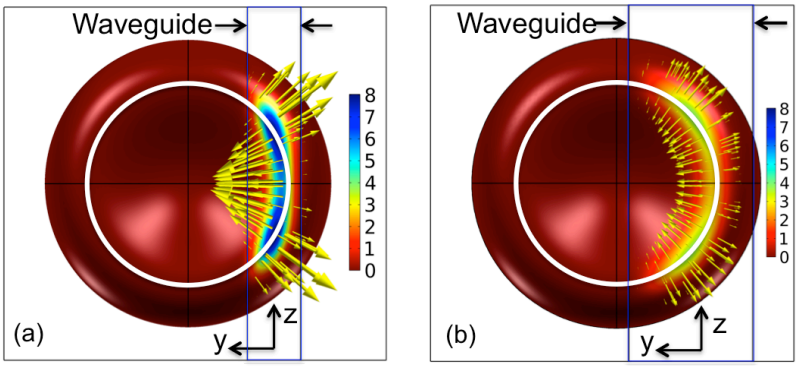

Supplementary Figure 6. Optical pressure distribution on a cell trapped at the stable position (i.e. $F_y = 0$), y = 2.1 μm and y = 1.8 μm for a) 1.3 μm and b) 3 μm wide waveguides, respectively. Pressure is shown in Pa for 15 mW of guided power. Arrows show direction of force density in yz-plane and the white circle indicates the bottom of the cell. The cells are seen from below, through the substrate and the waveguide. The scale for the arrows and colors are the same for both figures.

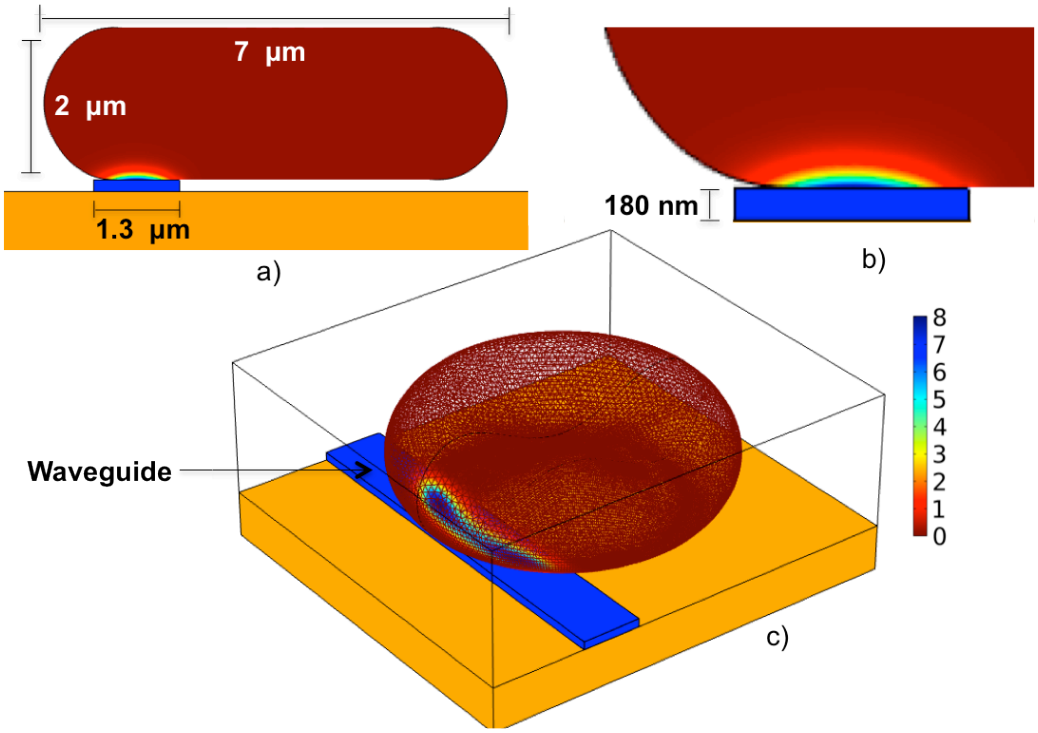

Supplementary Figure 7. Optical pressure distribution on a cell trapped at the stable position (i.e. F_y =0) on a 1.3 µm wide waveguide. The waveguide is shown blue and the substrate orange. a) Projected image of the cell as seen from the input face of the waveguide. b) Zoomed in on the contact area between cell and waveguide. c) 3D-view with wireframe rendering of the cell.

The force component F_z, pushing the cell forward, is significantly smaller than F_x and F_y (see Supplementary Fig 8). Thus, it was important to further reduce the numerical noise while computing F_z. Calculation of F_z from Eq. (2) was not successful as the numerical noise was too large. In the following, F_z is calculated from Eq. (4), which gave a significant reduction in noise. The force on the cell can be separated in two parts, with F_{z+} the force on the front half of the cell (facing the output and +z values) and F_{z-} the force on the back half (facing the input and -z values). The total force on the cell along the z-axis is thus $F_z = F_{z+} + F_{z-}$. The magnitude of this force is small as the signs of the two components are opposite, i.e. $F_z = |F_{z+}| - |F_{z-}|$, and thus makes the simulation prone to noise. The difference between the components, $F_{stretch} = F_{z+} - F_{z+}$ i.e. $F_{stretch} = |F_{z+}| + |F_{z-}|$, will act to stretch the part of the cell that is in the evanescent field. Supplementary Figure 8 shows F_z and $F_{stretch}$ as function of the offset of the cell from the centre of the waveguide. For small offsets, there is no stretching. As noted in the article, the stable position giving $F_y = 0$ is 2.1 µm for a waveguide width of 1.3 µm (see Figure 5b). For an offset corresponding to the stable position, the stretching force is relatively large, but only a small part of the cell is on the waveguide. It is the part of the cell overlapping with the evanescent field that is stretched, not the entire cell. The effect is thus to make the cell straight along the waveguide, rather than to increase the total length (along z-axis) of the cell, as observed experimentally (Supplementary Fig 3).

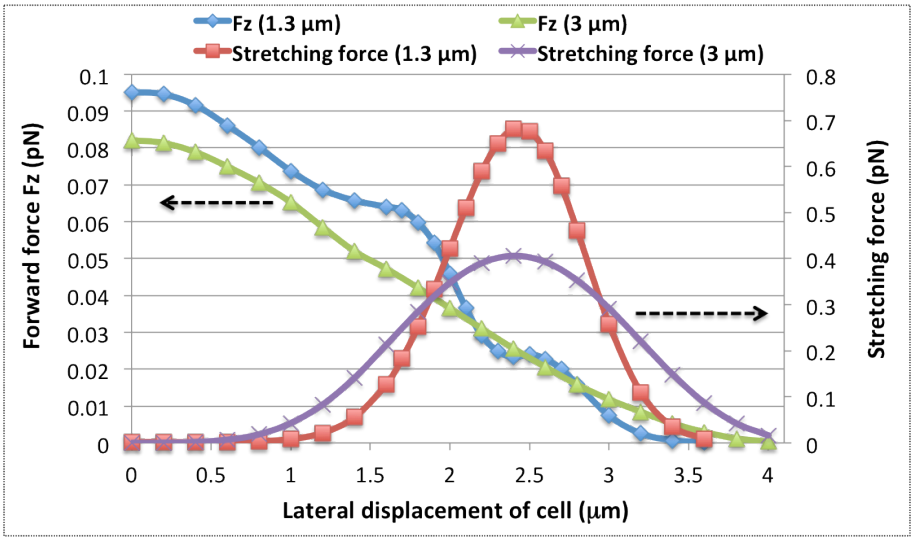

Supplementary Figure 8. Force F_z on the cell (left axis) and stretching force $F_{stretch}$ (right axis) as function of lateral offset along the y-axis. Results are shown for waveguide widths 1.3 and 3 µm for a guided power of 15mW.

Supplementary Figure 9 shows the torque on the cell relative to an axis of rotation (white line in Figure 7e-f) through the point of contact. For a positive torque, the cell is pressed down towards the substrate (see direction in Fig. 1a. A negative torque, which is found for an offset x > 2.6µm, will rotate (flip) the cell around the axis of rotation. The direction of the torque can be related to the distribution of pressure in Fig. 7f) and e). For an offset of x = 2.1µm (see Fig. 7f), most of the pressure is to the left of the axis of rotation and towards the centre of the cell, giving a positive torque. For an offset x = 3.0µm (see Fig. 7e), the pressure is to the right of the axis of rotation towards the edge of the cell, giving a (small) negative torque. As shown in Fig. 8, the torque is positive for the stable position (x = 2.1 µm) and, in general, the torque is positive unless the cell is almost entirely off the waveguide. Thus, the simulation predicts that the cell will be pressed down towards the substrate due to the positive torque and no flipping or rotation. This is also concurrent with our experimental observation where majority of cells were seen squeezed while their central donut could still be seen.

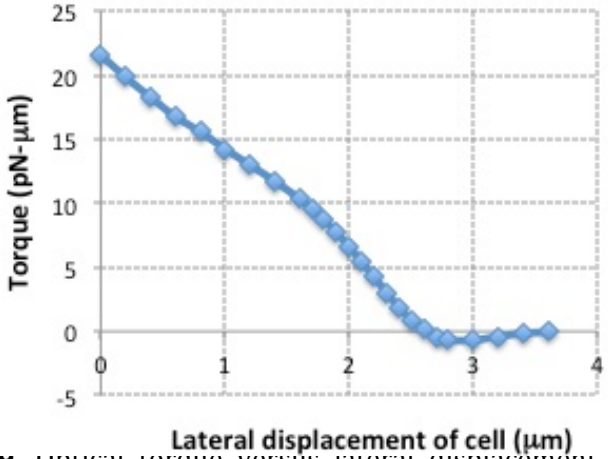

Supplementary Figure 9. Optical torque versus lateral displacement of the cell, with torque calculated relative to the axis of rotation shown in Fig. 7e-f).

Squeezing of red blood cells on waveguide

The effect of input power on the deformability of the blood cells was also studied as shown in Supplementary Fig. 10. The DI and the average DI of cell population increases with an increase of the input power, as indicated by Supplementary Figure 10a) and b), respectively. A constant input power should thus be chosen to measure the loss of cell deformability as a function of storage date.

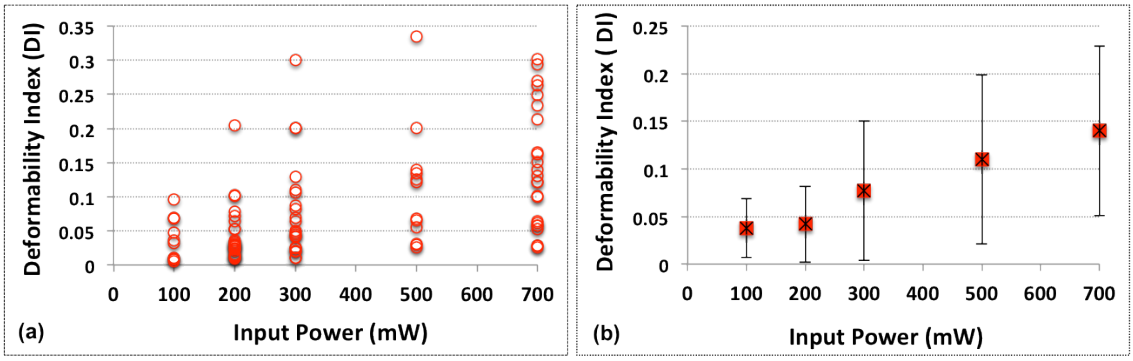

Supplementary Figure 10. a) Deformability of cells as function of input power. b) Average deformability index with error bars showing the standard deviation.

Supplementary references

1. Ahluwalia, B. S., et. al. Fabrication and optimization of Tantalum Pentoxide waveguides for optical micro-propulsion. *Proc. SPIE 7604, Integrated Optics: Devices, Materials, and Technologies XIV*, 76040W (2010).
2. Ahluwalia, B.S., McCourt, P, Huser, T., Helleso, O.G., Optical trapping and propulsion of red blood cells on waveguide surfaces. *Opt. Exp.* **18**, 21053-21061 (2010).
3. Brevik, I. Experiments in Phenomenological Electrodynamics and the Electromagnetic Energy-Momentum Tensor. *Phys. Rep.* **52**, 133-201 (1979).
4. Brevik, I. & Kluge. R. Oscillations of a water droplet illuminated by a linearly polarized laser pulse. *J. Opt. Soc. Am. B Opt. Phys*. **16**, 976-985 (1999).
5. Stallo computer cluster. Available from: http://www.notur.no/hardware/stallo/.
6. Evans, E.A., Fung, Y.C., Improved measurements of the erythrocyte geometry. Microvasc. Res., **4**, 335–347 (1972).
7. Dao, M., Lim C.T., Suresh. S. Mechanics of the human red blood cell deformed by optical tweezers. *J. Mech. Phys. Solids.* **51**, 2259-2280 (2003).
8. Park, Y.K. et. al. Refractive index maps and membrane dynamics of human red blood cells parasitized by Plasmodium falciparum. *Proc. Nat. Acad. Sci. U.S.A.* **105**, 13730-13735 (2008).
9. Gaugiran, S., Gétin, S., Fedeli, J., Colas, G., Fuchs, A., Chatelain, F., Dérouard J. Optical manipulation of microparticles and cells on silicon nitride waveguides. Opt. Exp., **13**, 6956-6963, (2005).
10. Jackson, J.D., Classical electrodynamics. 2nd ed., 1975, New York: Wiley. xxii, 848 p.
11. Barton, J.P., et al. Theoretical determination of net radiation force and torque for a spherical particle illuminated by a focused laser beam. J. Appl. Phys. **66**, 4594-4602, (1989).